https://doi.org/10.5194/essd-2021-309
Preprint. Discussion started: 20 October 2021

Open Access Earth System Science Data Discussions

A dataset of daily near-surface air temperature in China from 1979 to 2018

Shu Fang [1,2★], Kebiao Mao[1,3★], Xueqi Xia[2], Ping Wang[1,4], Jiancheng Shi[5], Sayed M. Bateni[6], Tongren Xu[7], Mengmeng Cao[1], Essam Heggy[8,9]

1.Institute of agricultural resources and regional planning, Chinese Academy of Agricultural Sciences, Beijing, 100081, China.

2. School of Earth Sciences and Resources, China University of Geosciences, Beijing, 100083, China. xiaxueqi@cugb.edu.cn

3. School of Physics and Electronic-Engineering, Ningxia University, Yinchuan 750021, China.

4. School of Surveying and Geo-Informatics, Shandong Jianzhu University, Jinan, 250100, China.

5. National Space Science Center, Chinese Academy of Sciences, Beijing, 100190, China. shijiancheng@nssc.ac.cn

6. Department of Civil and Environmental Engineering and Water Resources Research Center, University of Hawaii at Manoa, Honolulu, HI 96822, USA; smbateni@hawaii.edu

7. State Key Laboratory of Earth Surface Processes and Resource Ecology, School of Natural Resources, Faculty of Geographical Science, Beijing Normal University, Beijing 100875, China; xutr@bnu.edu.cn

8. Viterbi School of Engineering, University of Southern California, Los Angeles, CA 90089, USA; heggy@usc.edu

9. Jet Propulsion Laboratory, California Institute of Technology, Pasadena, CA 91109, USA.

Correspondence to: Kebiao Mao (maokebiao@caas.cn)

★ These authors contributed equally to this work.

Abstract: T_a (Near-surface air temperature) is an important physical parameter that reflects climate change. Although there are currently many methods to obtain the daily maximum (T_{max}), minimum (T_{min}), and average (T_{avg}) temperature (meteorological stations, remote sensing, and reanalysis data), these methods are affected by multiple factors. In order to obtain daily T_a data (T_{max}, T_{min}, and T_{avg}) with high spatial and temporal resolution in China, we fully analyzed the advantages and disadvantages of various existing data (reanalysis, remote sensing, and in situ data). Different T_a reconstruction models are constructed for different weather conditions, and we further improve data accuracy through building correction equations for different regions. Finally, a dataset of daily temperature (T_{max}, T_{min}, and T_{avg}) in China from 1979 to 2018 was obtained with a spatial resolution of 0.1°. For T_{max}, validation using in situ data shows that the root mean square error (RMSE) ranges from 0.86 ℃ to 1.78 ℃, the mean absolute error (MAE) varies from 0.63 ℃

https://doi.org/10.5194/essd-2021-309
Preprint. Discussion started: 20 October 2021

Open Access Earth System Science Data Discussions

to 1.40 ℃, and the Pearson coefficient (R^2) ranges from 0.96 to 0.99. For T_{min}, RMSE ranges from 0.78 ℃ to 2.09 ℃, the MAE varies from 0.58 ℃ to 1.61 ℃, and the R^2 ranges from 0.95 to 0.99. For T_{avg}, RMSE ranges from 0.35 ℃ to 1.00 ℃, the MAE varies from 0.27 ℃ to 0.68 ℃, and the R^2 ranges from 0.99 to 1.00. Furthermore, a variety of evaluation indicators were used to analyze the temporal and spatial variation trends of T_a, and the T_{avg} increase was more than 0.03 ℃/a, which are consistent with the general global warming trend. In conclusion, this dataset had a high spatial resolution and reliable accuracy, which makes up for the previous missing temperature value (T_{max}, T_{min}, and T_{avg}) at high spatial resolution. This dataset also provides key parameters for the study of climate change, especially high-temperature drought and low-temperature chilling damage, which is publicly available with the following DOI: https://doi.org/10.5281/zenodo.5502275 (Fang et al., 2021).

1. Introduction

T_a (Near-surface air temperature) is an important variable that reflects global climate change, and it significantly affects the cyclical conversion of energy and matter in all spheres of the earth (Gao et al., 2012, 2014). Obtaining accurate grid air temperature is helpful for research on urban heat island effects, the ecological environment changes, vegetation phenology development, crop yield fluctuation, and energy dynamic balance (Lin et al., 2012; Bolstad et al., 1998). In this study, T_a refers to the daily maximum (T_{max}), minimum (T_{min}), and average temperatures (T_{avg}) of daily near-surface air temperature, which are important input parameters for hydrological, environmental, and crop models (Han et al., 2020; He et al., 2020; Mostovoy et al., 2006; Schaer et al., 2004). They can accurately reflect the frequency and extent of the occurrence and development of extreme climate events (Zhang et al., 2017; Miao et al., 2016). With the increase in global warming, the temperature gradually increases and the extremely cold days and nights gradually shorten (Ding et al., 2006; Liao et al., 2020). However, the intensity and duration of extreme weather events are also increasing, and continuous bad weather in some years leads to frequent meteorological disasters (Ryoo et al., 2010). China is a country where extreme weather events frequently occur, which causes huge economic losses (Kharin et al., 2007; Kong et al., 2020). Therefore, it is essential to obtain the spatio-temporal changes of T_a for studying extreme weather events, meteorological disasters leading to agricultural production reduction.

https://doi.org/10.5194/essd-2021-309
Preprint. Discussion started: 20 October 2021

T_a is affected by many factors of the earth's system, resulting in frequent and complicated daily temperature fluctuations (Schwingshackl et al., 2018; Chen et al., 2014). At present, T_a is obtained mainly through three methods: monitoring T_a via meteorological stations, estimating T_a from T_s (land surface temperature) retrieved from remote sensing, and obtaining T_a through the assimilation model. The temperature with high time resolution can be obtained through the measurement of the meteorological station, which can avoid the influence of clouds and rain, preserving good data integrity, continuity, and accuracy. However, the number of meteorological stations is limited and unevenly distributed, especially for mountainous regions (Mao et al., 2008; Gao et al., 2018; Zhao et al., 2020). Most meteorological stations are located in sparsely populated areas far away from cities and cannot accurately monitor changes in urban temperature caused by the urban heat island effect (He and Wang, 2020). Moreover, owing to the aging of meteorological station equipment, the observation data may be incomplete. Although many interpolation methods, such as Kriging, Cubic Spline, and Inverse Distance Weight interpolations are available, the difference in density between stations has some impact on the interpolation accuracy (Tang et al., 2020; Tomasz et al., 2016; Tencer et al., 2011).

Satellite sensors can provide global coverage and high spatial resolution data, which can be used to estimate T_a. The estimation methods are mainly divided into five categories. The first method is the statistical regression method, which simulates the fluctuation of daily temperature by establishing a regression model between temperature and other parameters (Wen et al., 2020). The model parameters mainly include altitude, latitude and longitude, solar phase angle, and day length (Zhu et al., 2013; Zhang et al., 2015). The second method is the temperature vegetation index (TVX) method, which is a method for air temperature estimation based on the negative correlation between surface temperature and vegetation index (Xing et al., 2020). The third method is the energy balance method. It is generally considered that the sum of the net radiation and anthropogenic heat flux in the surface energy is equal to the sum of the surface sensible heat flux and latent heat flux to calculate the surface air temperature (Benali et al., 2012). The fourth method is the atmospheric temperature profile extrapolation method, which uses the vertical attenuation rate obtained from the atmospheric temperature profile to calculate the T_a (Wen et al., 2020). The fifth method is a machine learning method that uses polynomial regression or neural

https://doi.org/10.5194/essd-2021-309
Preprint. Discussion started: 20 October 2021


Open Access Earth System Science Data Discussions

network algorithms to improve T_a estimation errors (Mao et al, 2008; Wen et al., 2020). Sensors are susceptible to weather phenomena, such as clouds and rain, leading to missing data or reduced quality. In addition, these methods of inferring T_a are mostly suitable for clear sky conditions, which still need to be further expanded to establish an estimation model of T_s to T_a under different weather conditions.

In recent years, the reanalysis data generated by the global assimilation model has provided many datasets of geophysical parameters, including near-surface temperature, which overcome most of the above-mentioned problems caused by abnormal weather. The NCEP/NCAR reanalysis dataset was developed by the National Center for Environmental Prediction and the National Center for Atmospheric Research (1948.1–2021.9), with a time resolution of 6 h and a spatial resolution of 2.5° (Kobayashi et al., 2015). The ERA5 dataset was released by the European Center for Medium-Range Weather Forecast (ECMWF; 1950.1–2021.9), with a time resolution of 1 h, and a spatial resolution of 0.3° (Hersbach et al., 2020; Dee et al., 2011; Taszarek et al., 2021; Lei et al., 2020). The Princeton Forcing surface model dataset was developed by Princeton University (1948.1–2006.12), with a time resolution of 3 h and a spatial resolution of 1.0° (Deng et al., 2010). To improve the accuracy of regional data, some researchers have developed different types of forcing datasets for the Chinese region. The representative dataset is the China Meteorological Forcing Dataset (CMFD) released by the Institute of Tibetan Plateau Research, Chinese Academy of Sciences (1979.1–2018.12), with a time resolution of 3 h and a spatial resolution of 0.1° (He et al., 2010; Yang et al., 2010; Yang and He, 2019). However, the dataset does not provide daily maximum and minimum temperatures. The grid dataset of daily surface temperature in China (V2.0, CMA) was released by the China Meteorological Administration (1961.1–2021.9), with a spatial resolution of 0.5°. This dataset only includes the daily maximum, minimum, and average temperatures, and its spatial resolution is low and the accuracy of local areas needs to be further improved. Although reanalysis datasets can obtain global near surface air temperature data, there is a lack of T_{max}, T_{min} and T_{avg} dataset with high spatial resolution and high precision.

In order to obtain a long-term T_a (T_{max}, T_{min}, and T_{avg}) dataset with high spatial resolution in China based on the current reanalysis, remote sensing, and in situ data. We first analyze the

https://doi.org/10.5194/essd-2021-309
Preprint. Discussion started: 20 October 2021


Open Access Earth System Science Data Discussions

advantages and disadvantages of various existing data (reanalysis, remote sensing, in situ data, etc.). Then, different daily T_a reconstruction models are constructed for different weather conditions. It makes up for the previous methods which are most suitable for clear sky conditions and the insufficient estimation of all-weather conditions. We further improve data accuracy by building correction equations for different regions. Finally, a dataset of daily T_a (T_{max}, T_{min}, and T_{avg}) in China from 1979 to 2018 was obtained with a spatial resolution of 0.1°. The comparison with in situ data and the existing reanalysis dataset is made.

2. Study area

China has a vast territory, with great undulations on the earth's surface, and a wide range of climate changes. In order to improve the accuracy of T_a estimation, we divide China into six subregions shown in Figure 1 based on geographic location, altitude, rainfall, vegetation types and other natural environmental conditions. (I) The Northeastern Region is mainly including northeast China, which is located to the east of the Greater Khingan Range. This region is located in the temperate monsoon climate zone, the annual precipitation is 400–1000 mm and cumulative temperature is between 2500°C and 4000°C. (II) The North China region is located in the area north of the Qinling-Huaihe River and south of the Inner Mongolia Plateau. This region is mostly located in the temperate monsoon climate zone, the annual accumulated temperature is between 3000°C and 4500°C, with hot and rainy summers and cold and dry winters. (III) The Central Southern region is located south of the Qinling-Huaihe River and north of the tropical monsoon climate type. This region is located in the subtropical monsoon climate zone, the annual accumulated temperature is between 4500°C and 8000°C and the precipitation is mostly between 800 mm and 1600 mm. (IV) The Southern region is south of the Tropic of Cancer. This region is located in the tropical monsoon climate zone, the annual accumulated temperature is greater than 800°C, the annual minimum temperature is not less than 0°C, and there is no frost throughout the year. The annual precipitation mostly ranges from 1500 mm to 2000 mm. (V) The Northwest region is mainly distributed in the inland areas above 40° N latitude of China, located in the northwest of the Greater Khingan Range-Yin Shan-Ho–lan Mountains-Qilian Mountains line. It is far from the coast, water vapor transport is limited, and the annual precipitation is between 300 mm and 500 mm. Both the daily and the annual temperature differences are large, including

https://doi.org/10.5194/essd-2021-309
Preprint. Discussion started: 20 October 2021

Open Access Earth System Science Data Discussions

temperate desert, temperate grassy, and sub-frigid coniferous climates. (VI) The Qinghai–Tibet Plateau region mainly includes the Qinghai-Tibet Plateau, the Andes Mountains, Mount Everest, and other areas. This region is located in the plateau and mountainous climate zone, the annual accumulated temperature is lower than 2000°C, the daily temperature range is large, and the annual temperature range is small. This region has strong solar radiation, sufficient sunshine, and little precipitation.

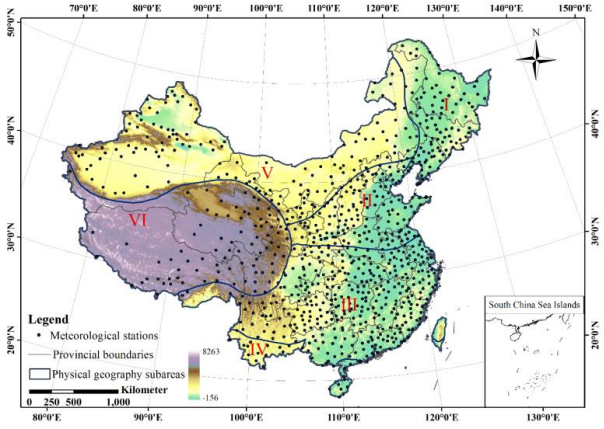

Figure 1. Scope map of the total study area and the six subregions. The black dots indicate the distribution locations of meteorological stations; blue frame lines indicate the sub-study area range, represented by I, II, III, IV, V, and VI.

3. Data

3.1 Reanalysis data

The reanalysis dataset contains driving factors of surface elements in a large area, which can provide highly complementary information and avoid data gaps and low pixel quality caused by abnormal weather conditions. This study primarily used the CMFD and ERA5 datasets as the reanalysis data sources.

CMFD data are a set of meteorological forcing datasets developed by the Institute of Tibetan Plateau Research, Chinese Academy of Sciences (He et al., 2020; Yang et al., 2010; Yang and He, 2019). They are mainly based on the Global Land Data Assimilation System (GLDAS) as a background dataset, using empirical knowledge algorithms and combining GLDAS with measured data to obtain temperature data with a spatial resolution of 0.1°. The CMFD dataset contains seven variables: 2-m air temperature, surface pressure, specific humidity, 10-m wind

https://doi.org/10.5194/essd-2021-309
Preprint. Discussion started: 20 October 2021


Open Access Earth System Science Data Discussions

speed, downward shortwave, and downward longwave radiation, and precipitation rate. The CMFD dataset covers the period from January 1979 to December 2018. In total, four types of time resolution products are provided every 3 h, daily, monthly and annual averages. At present, CMFD data are a comprehensive dataset with the longest regional time series and the highest spatial resolution in China. Many studies and analyses show that the dataset's accuracy is high enough to meet the application requirements (Zhang et al., 2019; Wang et al., 2017). Therefore, we use the 3-h temperature and daily temperature data of the CMFD to construct the T_a model and make evaluation with this product, respectively. CMFD dataset is available through the China National Qinghai-Tibet Plateau Science Data Center (http://data.tpdc.ac.cn/zh-hans/data/8028b944-daaa-4511-8769-965612652c49/, last access: 1 November 2020).

ERA5 data is the fifth-generation product of atmospheric reanalysis global climate data launched by the ECMWF, replacing the ERA-Interim reanalysis data that was discontinued on August 31, 2019 (https://cds.climate.copernicus.eu/cdsapp#!/search?type=dataset&text=ERA5, last access: 1 December 2020). ERA5 data is generated based on the Cy41r2 model of the integrated forecasting system which has benefited from the development of data assimilation, model simulation, and model physics in recent years, and is generated by absorbing more ground monitoring, aircraft weather observation, and radio detection data. Compared with ERA-Interim data, ERA5 was significantly improved, such as higher temporal and spatial resolution, more vertical mode levels, and added other parameter products. ERA5 provides timely and updated quality checks on the data, which is convenient for providing stable, real-time, and long-term climate information. ERA5 includes many meteorological elements, including 2-m air temperature, 2-m relative humidity, sea level pressure, sea surface temperature, and precipitation. Since the release of ERA5 reanalysis data, many researchers have tested its applicability and accuracy. The results show that the accuracy of the ERA5 is better than the ERA-Interim data, and the higher temporal and spatial resolutions are conducive to the precise description of regional atmospheres. The details of these improvements are convenient for studying changes in small-scale atmospheric environments (Meng et al., 2018; Mo et al., 2021; Hillebrand et al., 2021). Therefore, the temperature data in the ERA5 data is selected to reconstruct the T_a dataset.

https://doi.org/10.5194/essd-2021-309
Preprint. Discussion started: 20 October 2021

3.2 Meteorological station data

The meteorological station data from 1979-2018 were used in this study were employed to build a T_a model and make evaluations for existing datasets and new products. The measured data of meteorological stations are obtained from China National Meteorological Information Center (http://www.nmic.cn/site/index.html, last access: 1 November 2020), including the daily temperature data of China's surface climate (T_{max}, T_{min}, and T_{avg}), hourly air temperature, and land surface temperature data. In order to further improve the data quality, unified quality control was carried out on the in situ data. First set a fixed threshold to eliminate the overflow value. Secondly, we tested the time series of site data and eliminated abnormal and missing data due to instrument damage or bad weather. Finally, we checked the temporal and spatial consistency of the measurement data, delete the meteorological stations with location migration during the study period, and keep the temperature data of meteorological stations with long monitoring time and stable temperature values.

3.3 Supplementary data

China's daily near-surface temperature grid dataset was released by the CMA, with a spatial resolution of 0.5°. It is a grid dataset made for the daily maximum, minimum, and average temperatures in China (http://www.nmic.cn/site/index.html, last access: 11 April 2021). The CMA dataset was obtained by combining the daily temperature data monitored by meteorological stations and the digital elevation model (DEM) data generated by re-sampling with three-dimensional geospatial information through a thin-plate spline interpolation algorithm. The spatial resolution of the CMA data was 0.5°, which is used to make cross-validation.

Moderate Resolution Imaging Spectroradiometer (MODIS) is an important sensor in the Earth Observation System program, which is a medium-resolution imaging spectrometer mounted on the Terra and Aqua satellites. Terra is a morning orbiting satellite that passes through the equator at approximately 10:30 local time from north to south, and Aqua is an afternoon orbiting satellite that passes through the equator at approximately 1:30 local time from south to north. The Terra satellite has been in service since 1999, and the Aqua satellite has been in service since 2002. Since 2002, the surface temperature data can be obtained 4 times a day from MODIS data through

https://doi.org/10.5194/essd-2021-309
Preprint. Discussion started: 20 October 2021


Open Access Earth System Science Data Discussions

inversion calculation. In this study, we selected the MOD11A1 and MYD11A1 products, which can provide daily surface temperature data on a global scale with a spatial resolution of 1 km. To determine the locations of low-quality and missing values in pixels that are affected by cloud pollution and aerosols, MODIS provides quality control fields for each of its products, and quality control documents are mostly encoded in the binary form. MODIS data can be downloaded from the LAADS DAAC website (https://ladsweb.modaps.eosdis.nasa.gov/search/order, last access: 1 December 2020).

In addition to the above data, DEM data were used in this study. The Shuttle Radar Topography Mission (SRTM) DEM used in this study was a radar topographic mapping project jointly implemented by NASA and the National Imagery and Mapping Agency, which was implemented by the Space Shuttle Endeavour. The temperature data were regulated via topographical correction of SRTM DEM of 90-m resolution to eliminate the influence of topographical fluctuations on air temperature. SRTM DEM data can be obtained through the USGS network (http://www.gscloud.cn/search, last access: 10 February 2021).

4. Methodology

In currently, the T_{max}, T_{min}, and T_{avg} data can be provided by meteorological stations, other non-station locations or grid values were estimated by interpolation or indirect methods such as remote sensing. Owing to the limited number of meteorological stations and uneven distribution, it is difficult to guarantee the accuracy of T_{max}, T_{min}, and T_{avg} obtained through interpolation in some areas. Under rainfall and cloud cover weather conditions, it is impossible to estimate the air temperature from remotely sensed surface temperature data. Even in clear sky conditions, the formula for estimating near-surface air temperature is not universally applicable, which hinders the accurate development of the T_a dataset to a certain extent. Therefore, to obtain a T_a dataset with a high temporal and spatial resolution and long time series, it is necessary to build a reliable and robust T_a model to estimate T_{max} and T_{min}, and further improve the accuracy of T_{avg}. Consequently, the product can be more widely used for climate change and research on extreme weather events. Daily temperature changes are affected by many factors and are extremely sensitive to fluctuations in various weather phenomena. This study calculates T_{max} and T_{min} by distinguishing different weather conditions. First, the daily weather conditions were divided into

https://doi.org/10.5194/essd-2021-309
Preprint. Discussion started: 20 October 2021

the clear sky and non-clear sky conditions. Second, based on the physical process of daily temperature changes and combined with existing reanalysis data, in situ data, and remote sensing data, we construct T_{max} and T_{min} models under clear sky conditions. In non-clear sky weather conditions, a variety of methods are used to determine T_{max} and T_{min}. In order to further improve the accuracy of the data, a modified model is constructed according to the regional situation. More details are given in the following sections. The overall process of this study is illustrated in Fig. 2. The construction of the dataset was mainly divided into three steps: (1) The process of daily weather status determination, (2) the process of establishing T_a models under different weather conditions, and (3) data correction.

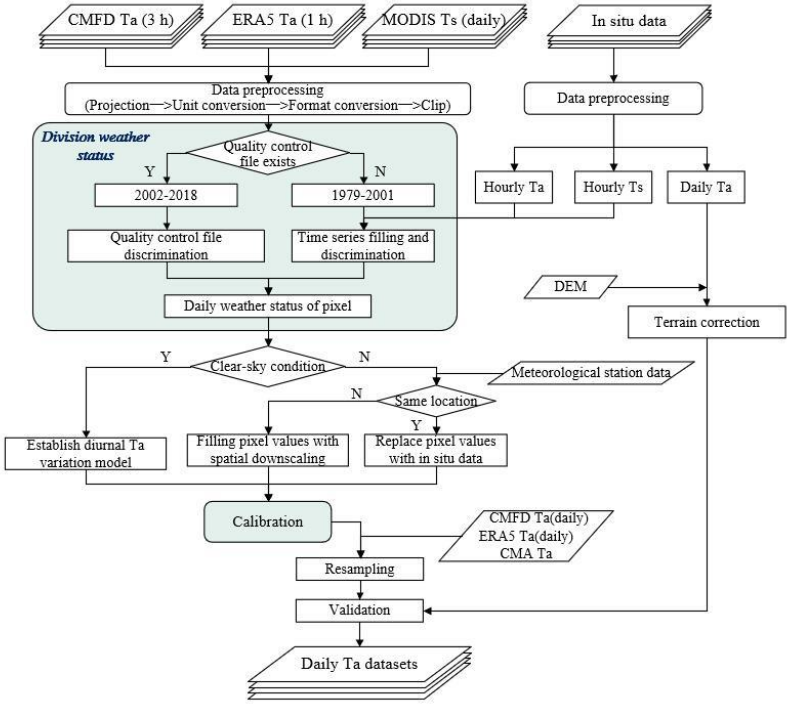

Figure 2. Summary flowchart of T_a dataset establishment.

4.1 Strategies for division of weather conditions and T_a estimation

4.1.1 Scheme for dividing weather conditions

Different weather conditions have different rules of temperature changes. In order to improve the estimation accuracy of the maximum and minimum temperature, we conduct specific calculations

https://doi.org/10.5194/essd-2021-309
Preprint. Discussion started: 20 October 2021


Open Access Earth System Science Data Discussions

by distinguishing daily weather conditions. Clouds and water vapor have a great influence on visible light and thermal infrared remote sensing. Many remote sensing data such as MODIS products generate quality control files for each pixel. Therefore, the quality control field of MODIS can be used to distinguish between clear sky and non-clear sky weather conditions. However, we can only obtain MODIS observation data four times a day since 2002, which cannot cover the time range involved in this study. Therefore, we divided the time series of this study into two periods: 1979–2001 and 2002–2018, and different methods are used for the two-time series to distinguish the daily weather status. For the study period from 2002 to 2018, we distinguished each pixel based on the MODIS quality control field. When the MODIS quality control of all four T_s corresponding to a pixel is in the clear sky condition, the pixel is judged to be in the clear sky condition, otherwise, it is judged to be in the non-clear sky condition.

For the study period from 1979 to 2002, we used the in situ, CMFD, and ERA5 data to determine the daily weather status. First, we filtered each pixel and divided it into two types: meteorological stations corresponding to pixels with and without weather status records. For pixels with weather status records, we used a large number of statistical discrimination methods to analyze the impact of abnormal weather phenomena on temperature fluctuations, which can facilitate the subsequent determination of pixels without weather status records. Statistical analysis shows that there is a significant difference in daily temperature fluctuations between clear sky and non-clear sky conditions, and non-clear weather conditions may cause abnormal temperature fluctuations. Therefore, we converted the judgment of the weather state into the abnormal judgment of the time and frequency of the occurrence T_{max} and T_{min} (The occurrence time of T_{max} and T_{min} is hereinafter cited as H_{max}, H_{min}). Specifically, when H_{max} and H_{min} occur abnormally or the temperature change is wavy, it is regarded as non-clear sky condition (Zhao and Duan, 2014; Ren et al., 2011). In other cases, they are regarded as clear sky states, and the position of each pixel is marked. Therefore, we needed to further fill the daily time series of each pixel to determine the weather state. In this study, we utilized two strategies to perfect the temperature series obtain the time and frequency of T_{max} and T_{min} for distinguishing the weather conditions. The specific implementation steps for determining weather conditions are shown in Figure 3.

https://doi.org/10.5194/essd-2021-309
Preprint. Discussion started: 20 October 2021

Open Access Earth System Science Data Discussions

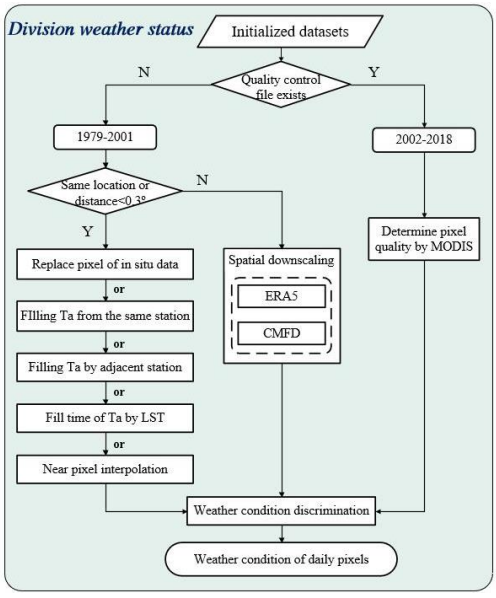

Figure 3. Summary flowchart for the classification of the weather conditions.

In the first strategy, when the pixel location had a corresponding meteorological station or when the Euclidean distance between adjacent stations was less than 0.3°, we fill in the gaps to improve the integrity and continuity of the time series. The time series filling process was as follows: (1) When there were missing values in the measured data at the site, there were no continuous missing values. In the case of the same spatial range, we use the average of the two times temperatures before and after the same site to fill in the missing values. (2) When the observation data of a site were missing continuously, in the case of the same time range, we filled it according to the time and frequency of the T_{max} and T_{min} occurrence of adjacent sites. This method is mainly based on the principle that the closer the distance between stations, the stronger the spatial consistency and correlation of temperature changes. (3) When the station data were continuously missing and the adjacent station data could not be filled, other relevant data were used for repair within the same time and space. In this study, we estimated the weather state based on the time and frequency of the T_{max} and T_{min} from the T_s monitored by the same station. This method theoretically originates from the approximate consistency between the daily variation ranges of T_s and T_a, and is suitable for situations where there are a large number of missing values and incomplete time series at meteorological stations and adjacent meteorological stations. Many studies have analyzed the

https://doi.org/10.5194/essd-2021-309
Preprint. Discussion started: 20 October 2021

correlation between the daily trend of T_a and T_s and found that they have strong consistency. The T_s retrieved by remote sensing satellites is also widely used to estimate T_a, which proves the reliability of determining the pixel weather state through the T_s time series (He et al., 2020; Yoo et al., 2018; Johnson and Fitzpatrick, 1977; Caesar et al., 2006; Mostovoy et al., 2006). (4) When there is no meteorological station at the pixel location and the distance from the meteorological station is less than 0.3°, we use the inverse distance weighting method to perform spatial interpolation on adjacent pixels. Determine the weather state by obtaining the time and frequency of each pixel's daily appearance of T_{max} and T_{min}.

The second strategy was to target areas where the distribution of sites was sparse and the Euclidean distance between two adjacent sites was greater than 0.3°. In order to make up for the insufficient coverage and uneven distribution of stations in these areas, this study uses hourly data from ERA5 to refine the time series of each pixel and distinguish the weather status. As there was a certain difference between the spatial resolution of ERA5 and this dataset, it was difficult to meet our demand for higher spatial resolution. Consequently, we developed an effective downscaling process based on the spatial correlation between ERA5 data and CMFD 3-h temperature data. The ERA5 data (with a spatial resolution of 0.3°) were spatially downscaled with the aid of CMFD data (with a spatial resolution of 0.1°). The downscaling process is illustrated in Fig. 4. First, quality control of the ERA5 and CMFD datasets was performed to eliminate temperature outliers. Second, ERA5 and CMFD data were matched according to time series and central latitude and longitude to construct pixel pairs. Subsequently, we weighted the high-resolution data to the low-resolution ERA5 data pixel by pixel. Finally, the weight was used to downscale the ERA5 data to the same spatial resolution of the CMFD. The ERA5 downscaling was computed using Eqs.1 and 2.

$$T_E(x_o,y_o)=\frac{T_C(x_o,y_o)}{\sum_{i=0}^{m}\sum_{j=0}^{n}T_C(x_i,y_j)}*T_E(x_m,y_n) \quad (1)$$

$$T_E(x_o,y_o)=\frac{T_M(x_o,y_o)}{\sum_{i=0}^{m}\sum_{j=0}^{n}T_M(x_i,y_j)}*T_E(x_m,y_n) \quad (2)$$

where T_E, T_C, T_M represents ERA5, CMFD, MODIS data, respectively. $T_E(x_o,y_o)$ is the temperature data after downscaling. $T_E(x_m,y_n)$ is the temperature data before downscaling. i, j are pixel coordinates. m, n are the pixel coordinates before downscaling.

https://doi.org/10.5194/essd-2021-309
Preprint. Discussion started: 20 October 2021

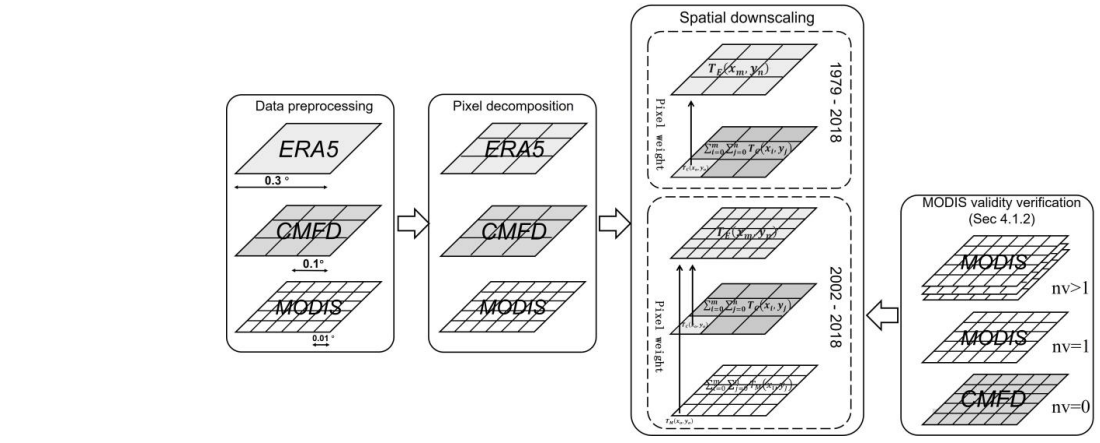

Figure 4. Flowchart for spatial downscaling, where nv represents the number of valid values.

4.1.2 T_{max} and T_{min} estimation under clear sky conditions

In addition to the temperature severe fluctuations caused by abnormal weather phenomena, the daily temperature changes under clear sky conditions have a certain regularity, periodicity, and asymmetry (Leuning et al., 1995; Johnson and Fitzpatrick, 1977). According to the similarity between the surface temperature and the diurnal variation trend of air temperature, a method of estimating T_a is established by the daily air temperature variation model. Verified by meteorological station data, this method is feasible (Du et al., 2020; Zhu et al., 2013; Perkins et al., 2007; Cesaraccio et al., 2001; Serrano-Notivoli et al., 2019). However, it is very complicated to use the surface temperature retrieved by remote sensing methods to estimate the changing trend of air temperature, and more parameters need to be input, and the relationship between T_s and T_a is not fixed. Therefore, it is difficult to unify the types and quantities of parameters, and it is difficult to ensure accuracy. As a result, we established a piecewise local sine function of temperature under clear sky conditions, which can simulate the change in T_a and calculate T_{max} and T_{min} (Mao et al., 2016; Jiang et al., 2010). First, according to the approximate periodicity of daily temperature changes and the asymmetry of H_{max} and H_{min}, we derive the T_a piecewise sine function of the adjacent regions of H_{max} and H_{min}, as shown in Eqs. 3 and 4. Among them, Eq. 3 is the T_{max} function and Eq. 4 is the T_{min} function. Secondly, it is similar to the method of filling the temperature time series when judging the weather state. By combining in-situ data and reanalysis data, the temperature sequence is improved and the H_{max} and H_{min} of each pixel are

https://doi.org/10.5194/essd-2021-309
Preprint. Discussion started: 20 October 2021

obtained. These H_{max} and H_{min} values are entered as parameters into the piecewise sine function. The CMFD 3-h data is used as T_a data, and each pixel H_{max} and H_{min} are used as time, and input into the piecewise sine function by the least square method for parameterization. We can obtain the values of A_t and B_t used to construct the piecewise sine function. The least squares method is a mathematical optimization technique, which uses the least square sum of residuals as the estimation standard for the best matching function. It is usually used in statistical models and is by far the most applicable and widely used parameter estimation method (Qiu and Jiang, 2021; Ge, 2015; Floyd and Braddock, 1984). Finally, H_{max} and H_{min} values were substituted into the derivation formula to obtain T_{max} and T_{min} as preliminary results for subsequent correction and analysis. By constructing a temperature model pixel by pixel to meet the temporal and spatial heterogeneity of each region.

$$T_{max} = A_t * \sin[\frac{(H_o - H_{max})\pi}{H_{max} - H_{min}} - \frac{\pi}{2}] + B_t \quad (3)$$

$$T_{min} = A_t * \sin[\frac{(H_o - H_{max})\pi}{24 - H_{max} + H_{min}} - \frac{\pi}{2}] + B_t \quad (4)$$

where H_{max} is the occurrence time of the daily maximum temperature. H_{min} is the occurrence time of the daily minimum temperature. H_o is the input time, and A_t and B_t are unknown parameters.

4.1.3 T_{max} and T_{min} estimation under cloudy-sky conditions

The daily temperature fluctuations in non-clear-sky conditions are relatively large, and there may be large-scale cooling or sudden temperature changes in a short period of time. Based on the spatial location information of each pixel, in situ data are the most reliable and representative data source. Therefore, if there are in situ data at the pixel location, the temperature data at the same time will be directly obtained from the site to replace the pixel values T_{max} and T_{min}. For the pixels corresponding to non-meteorological stations, similar to the method of spatial downscaling for the pixel positions of non-meteorological stations in the weather status judgment, we use ERA5 data to perform spatial downscaling with the assistance of CMFD data. By adding high spatial resolution MODIS data, the downscaling method is further expanded to improve the accuracy of each pixel. However, for the method of using remote sensing data to assist downscaling, we needed to consider the degree of influence of cloudy-sky weather phenomena. First, we performed effective value statistics on the MODIS data. When not all pixels of the MODIS data were valid,

https://doi.org/10.5194/essd-2021-309
Preprint. Discussion started: 20 October 2021


Open Access Earth System Science Data Discussions

the pixels with poor-quality or missing data were identified and removed. The corresponding time of the effective pixel was matched with the ERA5 data according to the nearby time to obtain the data weight for spatial downscaling. When the pixels in MODIS were invalid in 1 day, we used CMFD data for downscaling and finally obtained T_{max} and T_{min}. The downscaling process and the validity determination of MODIS data are shown in Figure 4, and the downscaling formulas are shown in Eqs. 1 and 2.

4.1.4 T_{avg} estimation

Usually, the calculation of average temperature is to use the temperature value observed every day to do an arithmetic average. If each pixel has hourly temperature data, the calculated daily average temperature is the most representative. Because it is difficult to obtain hourly data, people often use 4-hours temperature or directly use the maximum and minimum average values as the daily average temperature. In order to improve the accuracy of the average temperature as much as possible, we use the three-hour temperature data provided by CMFD and the maximum and minimum values calculated above to do an arithmetic average to get the daily average temperature. Finally, multiple linear regression correction was performed on the T_{avg} output value according to the in situ data to improve the accuracy (the linear correction method was the same as that described in Sect. 0), and the daily T_{avg} dataset was obtained.

4.2 T_a data calibration scheme

Surface temperature is sensitive to changes in altitude and is easily affected by the surrounding environment. For non-meteorological station pixels, we use interpolation to fill in the pixel values based on the principle of regional consistency. In order to improve the accuracy of pixel temperature at non-meteorological sites, we fully consider the influence of altitude on temperature. First, the in-situ T_a is unified to sea level according to the vertical rate of temperature drop. Then, the non-site pixels are interpolated according to the station data, and finally, the interpolated pixel values are restored to the corresponding elevation. This method can reduce the influence of altitude on temperature to a certain extent and improve the accuracy of the dataset. In this study, we used a uniform vertical temperature drop rate (γ), that is, for every 100 m increase in altitude, the atmospheric temperature drops vertically by 0.65°C, and vice versa. The height correction

https://doi.org/10.5194/essd-2021-309
Preprint. Discussion started: 20 October 2021

formula is given by Eq. 5 (He and Wang, 2020; Schicker et al., 2015; Wang et al., 2013).

$$T_{SL} = T_a - \gamma * (H_{SL} - H_a) \quad (5)$$

where T_{SL} is the sea level temperature, T_a is the temperature of the meteorological station, and H_{SL} is the sea level height, where the value of γ is approximately 0.0065°C/m.

Based on the jackknife method, 699 in situ stations across the country were divided into 140 verification points and 559 calibration points according to the ratio of in 20% and 80% to establish a multiple linear regression equation (Benali et al., 2012; Xu et al., 2017). From the preliminary accuracy results of the temperature change model in Sect. 0, it can be seen that although the overall accuracy was high, there is still the problem of abnormal temperature values of the model output data caused by the violent fluctuations in daily temperature changes. Further correction is required to reduce the deviation and improve the accuracy of the dataset. The data correction process is illustrated in Figure 5. For the abnormal temperature value, we replace the T_a at the pixel location with the observation T_a from the meteorological station, and performed the adjacent pixel temperature correction for the pixel without the meteorological station at the pixel location. The multiple linear regression method is used to perform multiple linear regression on the original temperature, and the stepwise regression relationship between the measured value of the station and the fitted value of the corresponding pixel is established. Then calculate the predicted value of the regression temperature according to the regression equation, and obtain the temperature residual value by calculating the observed value and the predicted value. The residual value and the predicted value are spatially added to obtain the final corrected temperature (Cristobal et al., 2006). The modified expression is shown in Eq. 6.

$$V(x, y) = \hat{m}(x, y) + \hat{\varepsilon}(x, y) \quad (6)$$

where x and y are the numbers of rows and columns of pixels, respectively, $V(x, y)$ is the correction value of the regression equation, $\hat{m}(x, y)$ is the regression prediction value of air temperature, and $\hat{\varepsilon}(x, y)$ is the residual value.

https://doi.org/10.5194/essd-2021-309
Preprint. Discussion started: 20 October 2021

Open Access Earth System Science Data Discussions

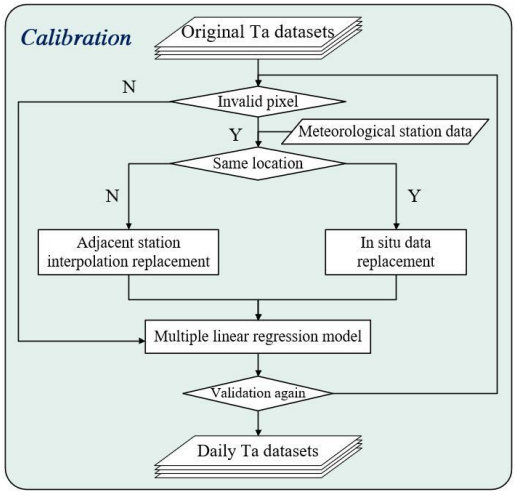

Figure 5. Flowchart for calibration of T_a model data.

4.3 Evaluation metrics

To verify the accuracy of this dataset, we first verified the accuracy of the original temperature dataset and the corrected dataset in this study with the in situ data. A scatter diagram was used to compare the results before and after validation. The scatter diagram represents the overall distribution and aggregation of the data and can intuitively convey accurate information of the data. Further, to better evaluate the accuracy of this dataset, we selected areas with uniform surface types and flat terrain under clear skies as the comparative study area and compared this product with the existing datasets. We selected three indicators as metrics to measure the accuracy of variables: R^2, MAE, RMSE.

We compared T_{max} and T_{min} with ERA5 data and CMA data. It is worth noting that the ERA5 reanalysis dataset is an hourly temperature grid dataset, so we obtain the highest and lowest temperature values of ERA5 by constructing a local sine function similar to the previous section, and further calculate the average daily temperature. The accuracy of T_{avg} products in this study is verified with ERA5 data, CMA data, and CMFD daily temperature data. Since the spatial resolution of CMA is 0.5°, in order to facilitate comparison, we resample the spatial resolution of all datasets to 0.5°.

https://doi.org/10.5194/essd-2021-309
Preprint. Discussion started: 20 October 2021

4.4 Analysis of the T_a series trend

We not only compared the output T_a data with the in situ data, but also assessed the climate change trends of T_{max}, T_{min}, and T_{avg} in various regions of China, and further tested the effectiveness and regional applicability of the dataset through various climate variables. This study used four temperature indexes (TXx, TNn, TX90p, and TN10p) to analyze the trends of T_{max} and T_{min} extreme temperature changes each year. Specifically, TXx (TNn) abnormality refers to the difference between the sum of monthly T_{max} (T_{min}) and the multi-year average of monthly T_{max} (T_{min}) in each year. The multi-year period of this study is 40 years. In addition, linear regression was performed on the TXx (TNn) anomaly to analyze the inter-annual variation trend. The TX90p (TN10p) arranged the daily T_{max} (T_{min}) of each month during the study period in ascending order of temperature, and we selected the portions with more than 90% (less than 10%) correlation with the number of days in each year.

To study the spatiotemporal variation trend of T_{avg}, we used linear regression analysis (K), correlation coefficient analysis (R), and T-test (Du et al., 2020; Yan et al., 2020; Cao et al., 2021). The interannual change rate and correlation of T_{avg} were calculated by K and R, and the formula is given by Eqs. 7 and 8, respectively. We performed a two-tailed significance test on the T-test to quantify the significance of the temperature and time-series changes (Eq. 9).

$$K = \frac{n\sum_{i=1}^{n}(iT_i) - \sum_{i=1}^{n} i \sum_{i=1}^{n} T_i}{n\sum_{i=1}^{n} i^2 - (\sum_{i=1}^{n} i)^2} \tag{7}$$

$$R = \frac{n\sum_{i=1}^{n}(iT_i) - \sum_{i=1}^{n} i \sum_{i=1}^{n} T_i}{\sqrt{n\sum_{i=1}^{n} i^2 - (\sum_{i=1}^{n} i)^2} * \sqrt{n\sum_{i=1}^{n} T_i^2 - (\sum_{i=1}^{n} T_i)^2}} \tag{8}$$

$$T\_test(R) = \frac{R\sqrt{n-2}}{\sqrt{1-R^2}} \tag{9}$$

where n represents the total number of years of the time series length, i represents the year, and T_i represents T_{avg} in the i-th year. $K > 0$ indicates that the temperature is increases within the time series, and $K < 0$ indicates that the temperature is decreases within the time series.

5. Results

5.1 Accuracy verification before calibration

According to the six subregions divided in Fig. 1, comparative analysis of this product (T_{max}, T_{min}

https://doi.org/10.5194/essd-2021-309
Preprint. Discussion started: 20 October 2021

Open Access Earth System Science Data Discussions

and T_{avg}) based on in-situ data are made respectively. Fig. 6 shows the accuracy scatter plot between the original data of T_{max} and the in situ data. The R^2 fluctuated from 0.91 to 0.99, the MAE ranged from 1.69 °C to 2.71 °C, and the RMSE ranged from 2.15 °C to 3.20 °C. Fig. 7 shows the accuracy scatter plot of T_{min}. The R^2 fluctuated from 0.93 to 0.97, the MAE ranged from 1.34 °C to 2.17 °C, and the RMSE fluctuated from 1.68 °C to 2.79 °C. Fig. 8 shows the accuracy scatter plot of T_{avg}. The R^2 fluctuated between 0.97 and 0.99, the MAE ranged from 0.58 °C to 0.96 °C, and the RMSE fluctuated from 0.86 °C to 1.60 °C. It can be seen from Figs. 6, 7, and 8 that the R^2 of T_{max}, T_{min}, and T_{avg} and the temperature measured at the meteorological station were all greater than 0.90. In general, our method performed well in estimating the daily temperature values. However, due to the impact of complex changes in weather, the distribution of temperature values on certain days is more discrete, especially in the study areas V and VI. Further corrections are needed to reduce errors and improve the accuracy of the dataset.

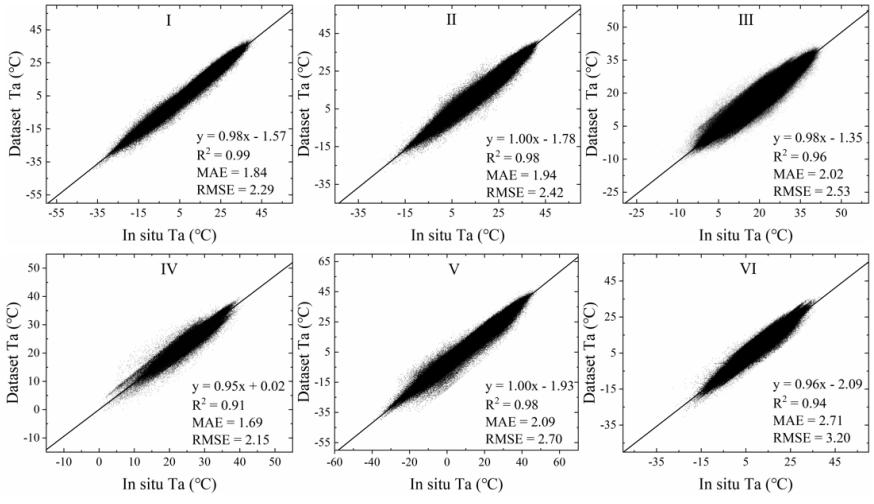

Figure 6. Scatter diagrams of the T_{max} output from the T_a model against ground station data; the statistical accuracy measures (R^2, MAE, and RMSE) are also indicated.

https://doi.org/10.5194/essd-2021-309
Preprint. Discussion started: 20 October 2021

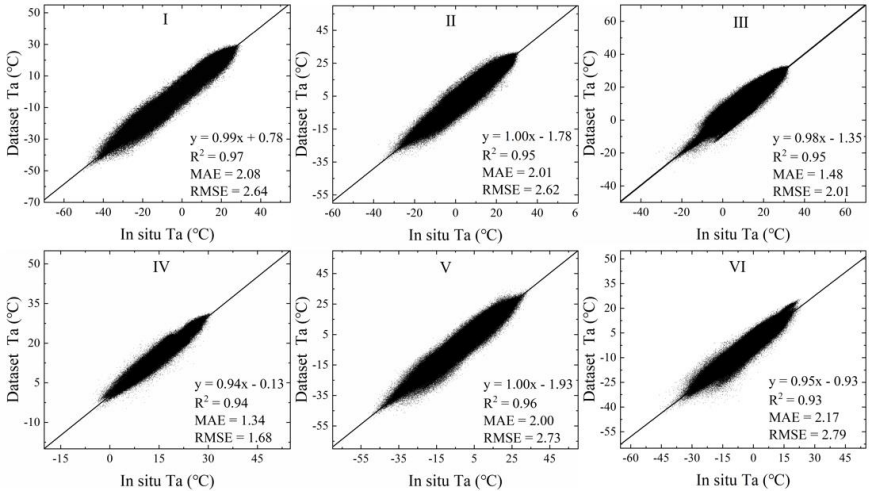

Figure 7. Scatter diagrams of the T_{min} output from the T_a model against ground station data; the statistical accuracy measures (R^2, MAE, and RMSE) are also indicated.

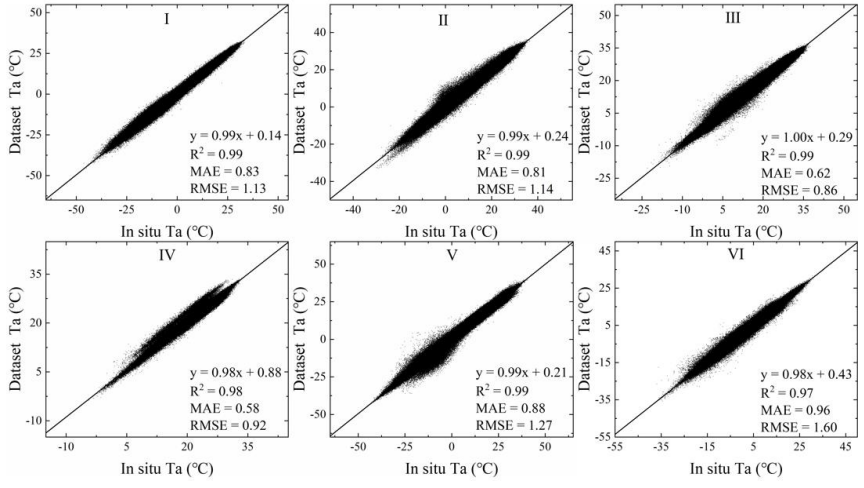

Figure 8. Scatter diagrams of the T_{avg} output from the T_a model against ground station data; the statistical accuracy measures (R^2, MAE, and RMSE) are also indicated.

5.2 Accuracy verification after calibration

The temperature was further corrected using the linear correction method. The data verification results of T_a after correction are shown in Figs. 9, 10, and 11. The results showed that the corrected data had a higher consistency with the in situ data. The fitted and observed temperatures were linearly distributed and gradually approached the regression line, and the outliers were greatly

https://doi.org/10.5194/essd-2021-309
Preprint. Discussion started: 20 October 2021


Open Access Earth System Science Data Discussions

reduced. Fig. 9 shows the corrected scatter plot of T_{max} for each study area. The R^2 fluctuated from 0.96 to 0.99, and the MAE ranged from 0.63 °C to 1.40 °C, the RMSE fluctuated from 0.86 °C to 1.78 °C. Fig. 10 shows the corrected scatter plot of T_{min} for each study area. The R^2 fluctuated between 0.95 and 0.99, and the MAE ranged from 0.58 °C to 1.61 °C, the RMSE fluctuated from 0.78 °C to 2.09 °C. Fig. 11 depicts the corrected scatter plot of T_{avg} in each study area, where R^2 fluctuated between 0.99 and 1.00, the MAE ranged from 0.27 °C to 0.68 °C, the RMSE fluctuated from 0.35 °C to 1.00 °C. The results showed that the distribution of numerical points in each area after the correction was denser, mostly concentrated near the 1:1 line, and the degree of clustering with the measured data was higher than before calibration. When we performed a detailed analysis of the daily temperature in the six study areas, we found that the accuracy measurement values differed greatly between the east and west. For example, the accuracy error of study area IV is small, and the accuracy error of study area VI and V is large, which may be affected by the regional topography and the distribution of meteorological stations. The IV study area is located in the tropical monsoon climate zone, affected by latitude and topography, the temperature is relatively high throughout the year. Moreover, the area is located in the eastern part of China with densely distributed meteorological stations and relatively flat terrain. Linear correction can significantly improve the agreement between the estimated value and the observed value. The study areas VI and V have higher RMSE. They are located in the Qinghai-Tibet Plateau in southwest China and Xinjiang in the northwest. Such areas have similar characteristics, such as high altitude, large spatial heterogeneity, and few meteorological stations. It shows that the temperature has strong spatial heterogeneity. In general, the corrected dataset has higher accuracy, satisfies the spatial heterogeneity of different regions, and better estimates the temperature under different weather conditions.

https://doi.org/10.5194/essd-2021-309
Preprint. Discussion started: 20 October 2021

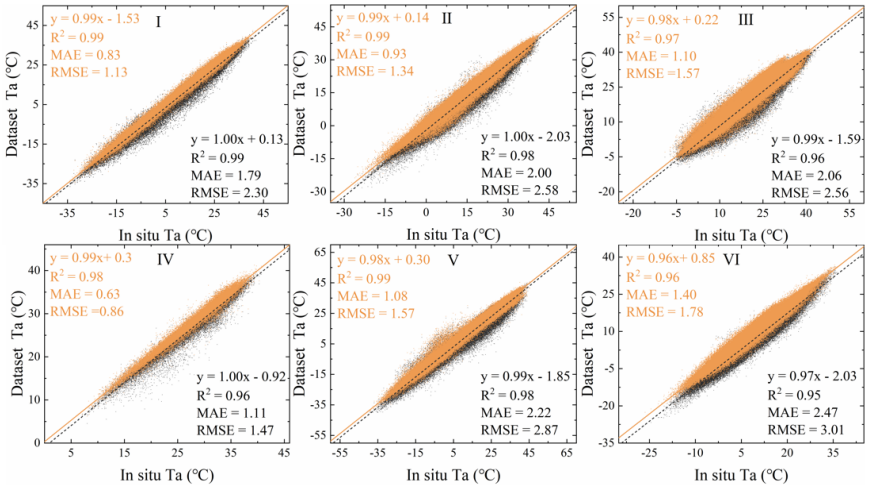

535 Figure 9. Scatter diagrams of the original T_{max} and reconstructed results versus their corresponding ground station data in six natural subregions (I, II, III, IV, V, and VI). The gray points indicate low-quality pixel values in the original T_{max} data, and the orange points represent the values in the after-calibrated T_{max} dataset, and the statistical accuracy measures (R^2, MAE, and RMSE) are also indicated.

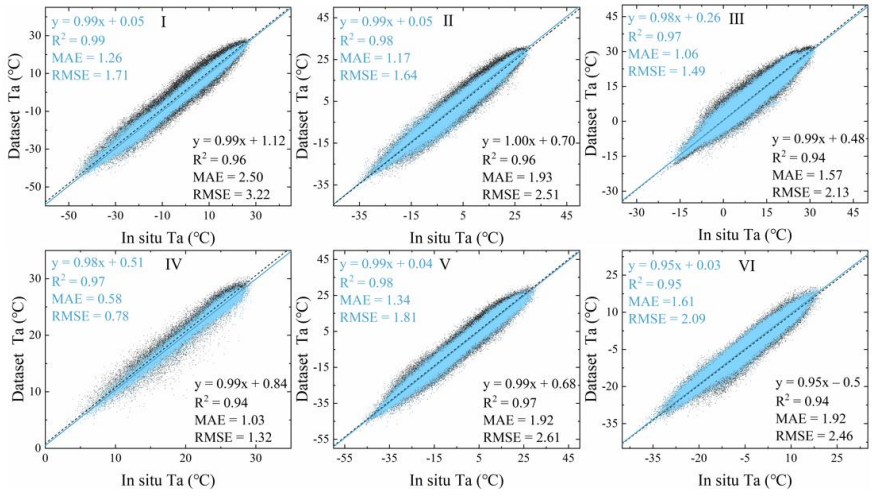

540 Figure 10. Scatter diagrams of the original T_{min} and reconstructed results versus their corresponding ground station data in six natural subregions (I, II, III, IV, V, and VI). The gray points indicate low-quality pixel values in the original T_{min} data, and the blue points represent the values in the after-calibrated T_{min} dataset, and the statistical accuracy measures (R^2, MAE, and RMSE) are also indicated.

https://doi.org/10.5194/essd-2021-309
Preprint. Discussion started: 20 October 2021

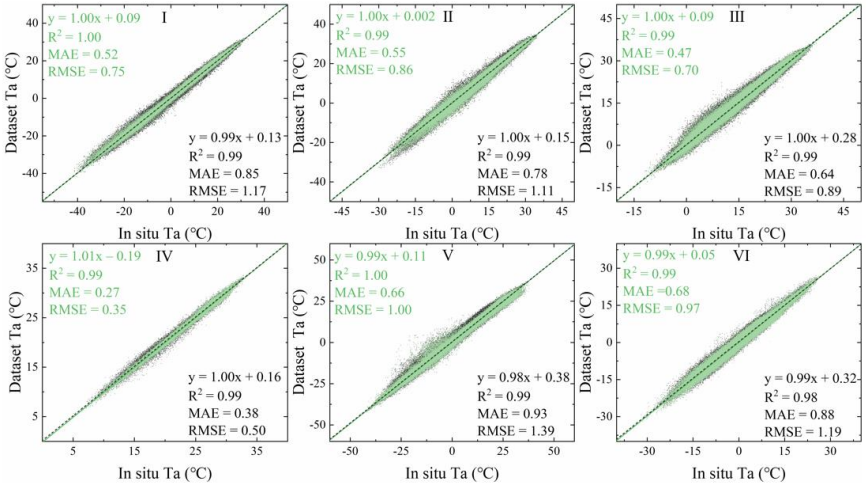

Figure 11. Scatter diagrams of the original T_{avg} and reconstructed results versus their corresponding ground station data in six natural subregions (I, II, III, IV, V, and VI). The gray points indicate low-quality pixel values in the original T_{avg} data, and the green points represent the values in the after-calibrated T_{avg} dataset, and the statistical accuracy measures (R^2, MAE, and RMSE) are also indicated.

To further verify the robustness and accuracy of this product, Table 1 shows the cross-validation results of this product and other datasets, and the mean average precision (MAP) of each region. It can be seen from the table that this product has a high regional consistency with other datasets. Study area IV located in the tropical monsoon climate zone has higher accuracy, while study area VI located in the Qinghai-Tibet Plateau region of China has lower data accuracy. This may be because the reanalysis dataset is also affected by the number and distribution of meteorological stations, and the spatial heterogeneity. The accuracy and robustness of the product has been confirmed from another angle. The accuracy comparison of each area shows that this product has higher accuracy and spatial representation than other datasets. R^2 is closer to 1, and both MAE and RMSE remain low. Through the accuracy evaluation and data comparison between this product and the existing dataset, it is found that our product has a better temperature estimation of each area, and the overall accuracy and accuracy of the dataset is higher.

Table 1. Cross-validation results of this product and other datasets.

Temp. Type	Index	Data	I	II	III	IV	V	VI	MAP
		ERA5	0.99	0.97	0.94	0.94	0.97	0.94	0.96

https://doi.org/10.5194/essd-2021-309
Preprint. Discussion started: 20 October 2021

MAX	R^2	CMA	1.00	0.95	0.95	0.98	0.99	0.90	0.96
		DATASET	0.99	0.99	0.97	0.98	0.99	0.96	0.98
	MAE	ERA5	1.05	1.25	1.47	0.99	1.53	1.99	1.38
		CMA	0.67	1.28	1.28	0.63	0.81	1.58	1.04
		DATASET	0.73	0.94	1.07	0.62	1.02	1.40	0.96
	RMSE	ERA5	1.69	1.52	2.14	1.68	1.91	2.30	1.87
		CMA	0.99	1.80	1.76	0.83	1.22	2.79	1.57
		DATASET	1.03	1.14	1.37	0.81	1.57	1.78	1.28
MIN	R^2	ERA5	0.96	0.95	0.96	0.95	0.97	0.90	0.95
		CMA	0.99	0.97	0.96	0.98	0.99	0.90	0.97
		DATASET	0.99	0.98	0.97	0.97	0.98	0.95	0.97
	MAE	ERA5	1.68	1.28	1.48	1.00	1.48	2.09	1.50
		CMA	0.85	1.24	1.18	0.46	0.98	2.23	1.16
		DATASET	1.13	1.14	1.04	0.57	1.34	1.41	1.10
	RMSE	ERA5	1.95	1.98	1.73	1.32	2.21	2.34	1.92
		CMA	1.19	1.99	1.72	0.63	1.47	2.80	1.63
		DATASET	1.31	1.60	1.49	0.74	1.61	2.05	1.47
AVG	R^2	CMFD	0.99	0.99	0.98	0.99	0.97	0.98	0.98
		ERA5	0.98	0.97	0.97	0.99	0.97	0.97	0.98
		CMA	1.00	0.97	0.96	0.99	0.99	0.91	0.97
		DATASET	0.99	0.99	0.98	0.99	0.98	0.98	0.99
	MAE	CMFD	0.46	0.49	0.44	0.30	0.53	0.89	0.52
		ERA5	0.50	0.52	0.48	0.45	0.70	0.73	0.56
		CMA	0.59	1.07	1.09	0.41	0.79	1.34	0.88
		DATASET	0.51	0.56	0.53	0.27	0.65	0.67	0.53
	RMSE	CMFD	0.60	1.19	0.75	0.41	1.26	1.17	0.90
		ERA5	0.57	1.17	0.71	0.52	1.24	1.15	0.89
		CMA	0.88	1.30	1.30	0.54	1.23	1.64	1.15
		DATASET	0.65	0.79	0.70	0.35	1.20	1.06	0.79

5.3 Application of the product for trend analysis

We analyze temperature changes in various regions of China through extreme climate indexes and change trend values to further test the validity and regional applicability of the dataset, as shown in Figs. 12 and 13, which show that the TXx anomalies and TNn anomalies are consistent in the regional change trend. Although the annual anomalies fluctuated during the study period, they gradually changed from negative to positive. This confirmed that the temperature fluctuated and increased, and the T_{max} and T_{min} gradually increased, which is consistent with the global warming trend. The average temperature rise of TXx anomalies in each study area was 0.42°C/a, and the

https://doi.org/10.5194/essd-2021-309
Preprint. Discussion started: 20 October 2021

570 average temperature rise of TXx anomalies was 0.47°C/a. The histograms in Figs. 12 and 13 show that the number of warm days and cold nights fluctuates increasing and decreasing trend, respectively. In addition, there are similarities in the change trends between warm days and cold nights. For example, in 1980, under the continuous influence of strong cold air in the north, low-temperature weather occurred continuously in most areas of China, and many areas experienced
575 low-temperature disasters, which leads to a decrease in the number of warm days and an increase in the number of cold nights. In 2015, 2016, and 2017, the temperature continued to rise, with high temperatures that occur once in decades. This is closely related to the severe El Niño events that occurred in 2015 and 2016, the impact of the subtropical high in 2017, and the overall global warming trend. At the same time, there has been an increase in the number of warm days and a
580 decrease in the number of cold nights. Meteorological events can indirectly verify the accuracy of this product, indicating that the corrected data can be used to analyze long-term temporal and spatial changes in temperature.

In order to further analyze the change rate and regional differences of T_{avg} during the study period, we conducted an analysis of the temperature change rate (K), correlation coefficient (R),
585 and significance test of the correlation coefficient (T-test(R)). As shown in Figure 14 (a) and (a'), T_{avg} in most regions of China showed a weak positive warming trend, accounting for 92.13% of the total, and the average temperature of T_{avg} in each region was rising by 0.03°C/a. Through the analysis of the R in Figure 14 (b) and (b'), it is observed that they show a strong correlation in the area of 48.77% and a correlation in the area of 84.06%, which shows that there is a high correlation
590 between temperature changes and time. Figure 14 (c) and (c') show that after performing a significance test on the R between temperature and time, 83.17% of the area passed the 95% significance test, and 75.23% of the area passed the 99% significance test, which shows that the correlation between temperature and time development is significant.

https://doi.org/10.5194/essd-2021-309
Preprint. Discussion started: 20 October 2021

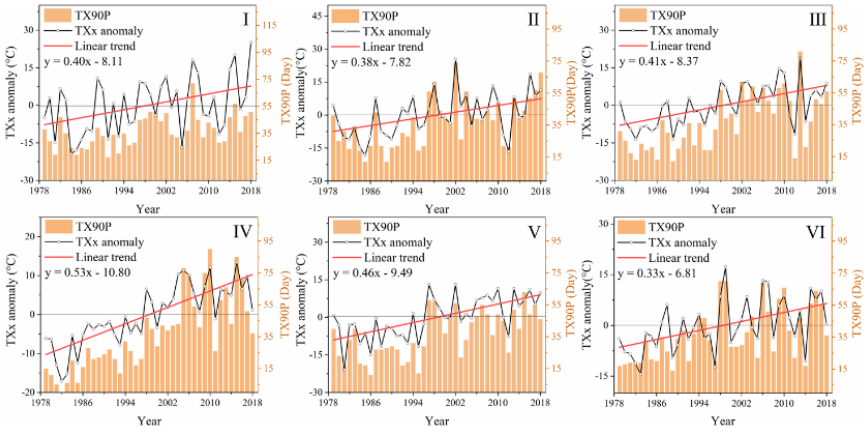

595 Figure 12. Multi-axis diagram of TXx anomaly, TX90p, and T_{max} linear trend graphs. The broken black line represents TXx anomaly, the red line represents the linear regression of the TXx anomaly, and the orange histogram represents the TX90p change trend.

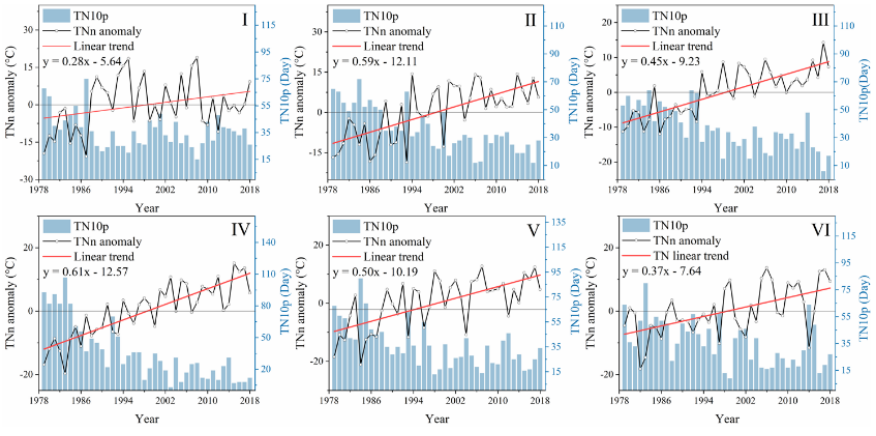

Figure 13. Multi-axis diagram of TNn anomaly, TN10p, and T_{min} linear trend graphs. The broken black line

600 represents TNn anomaly, the red line represents the linear regression of the TNn anomaly, and the blue histogram represents the TN10p change trend.

https://doi.org/10.5194/essd-2021-309
Preprint. Discussion started: 20 October 2021

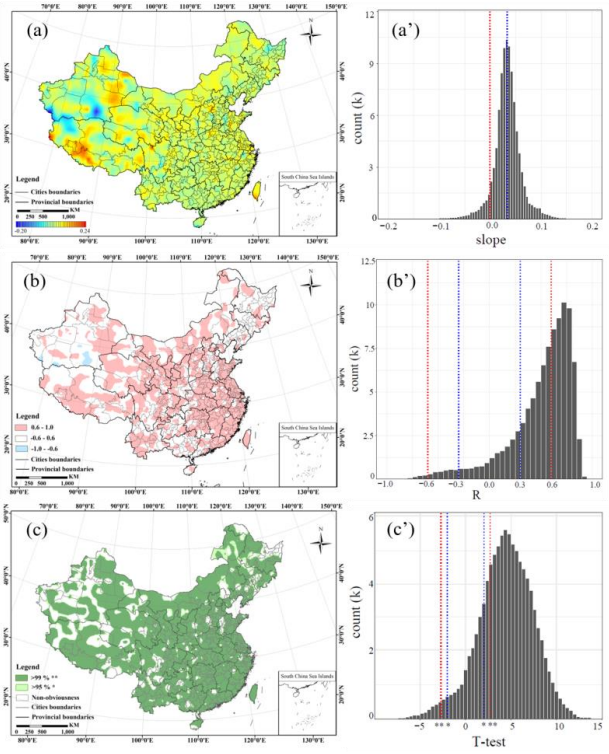

Figure 14. Multi-year climate change trends in T_{avg}. (a) K, calculated by Eq. 7; (b) R between temperature change and time series development, calculated by Eq. 8; (c) T-test (R), calculated by Eq. 9. (a'), (b') and (c') respectively represent the distribution of pixel values in the corresponding (a), (b) and (c) spatial images.

6. Data availability

The daily T_a products at 0.1° resolution from 1979 to 2018 are freely available to the public in the tif format at https://doi.org/10.5281/zenodo.5502275 (Fang et al., 2021), which are distributed under a Creative Commons Attribution 4.0 License.

7. Code availability

We are finishing and improving the code. If the paper is accepted, the code will be made public soon.

8. Conclusions

T_a is an indispensable variable for global climate change research. Therefore, it is very important for how to obtain high-precision and high-temporal resolution air temperature data products.

https://doi.org/10.5194/essd-2021-309
Preprint. Discussion started: 20 October 2021

Many researchers have made a lot of efforts, and have produced some datasets through different data sources for the global or local region. But with the need for refinement of research, we need to further improve the accuracy and spatio-temporal resolution. Based on the full analysis of the advantages and disadvantages of various datasets and data sources, this study integrates various data sources, such as in-situ data, remote sensing data, and reanalysis data, and proposes a reconstruction model of T_a under a clear sky and non-clear sky weather conditions, respectively. A multiple linear regression model was used to further improve the accuracy of the data, and we obtained a new set of grid high-resolution daily temperature datasets in China from 1979 to 2018. For T_{max}, validation using in situ data shows that the RMSE ranges from 0.86 ℃ to 1.78 ℃, the MAE varies from 0.63 ℃ to 1.40 ℃ and the R^2 ranges from 0.96 to 0.99. For T_{min}, RMSE ranges from 0.78 ℃ to 2.09 ℃, the MAE varies from 0.58 ℃ to 1.61 ℃ and the R^2 ranges from 0.95 to 0.99. For T_{avg}, RMSE ranges from 0.35 ℃ to 1.00 ℃, the MAE varies from 0.27 ℃ to 0.68 ℃ and the R^2 ranges from 0.99 to 1.00. Furthermore, we verified the T_a dataset with the existing reanalysis dataset and found that the proposed dataset has credibility and accuracy. Moreover, based on the particularity of geographic climate change in different regions, we used four extreme climate indicators (TXx and TNn anomalies, TX90p, and TN10p) and three climate change indices (K, R, and T-test) to analyze the trend changes of T_{max}, T_{min}, and T_{avg}, respectively. In summary, the temperature in most regions of China had been gradually increasing. The number of cold nights and warm days gradually decreased and increased, respectively, and the T_{max} and T_{min} gradually increased, which is consistent with the general trend of global warming.

However, due to various factors, the weather may occasionally change drastically, such as hail. Historical data cannot provide more specific weather information, especially in areas where there are no meteorological stations, it is difficult to refine past data. However, in future research, we need to consider more meteorological satellite data, especially geostationary meteorological satellites, which will help improve the accuracy of surface temperature datasets.

https://doi.org/10.5194/essd-2021-309
Preprint. Discussion started: 20 October 2021

Author contributions. SF and KM designed the research, developed the methodology and wrote the manuscript; and XX, PW, JS, SMB, TX, MC and EH revised the manuscript.

Competing interests. The authors declare no conflicts of interest.

Acknowledgements. The authors thank the China Meteorological Administration for providing CMA data and the ground measurements data, the Institute of Tibetan Plateau Research, Chinese Academy of Sciences for providing CMFD dataset, and the NASA Earth Observing System Data and Information System for providing the MODIS LST and DEM data. We also thank the ECMWF for providing the climate reanalysis data.

Financial support. This work was supported by the Second Tibetan Plateau Scientific Expedition and Research Program (STEP)"Dynamic monitoring and simulation of water cycle in Asian water tower area" (grant no. 2019QZKK0206), the National Key Project of China (grant no. 2018YFC1506602), the National Natural Science Foundation of China (grant no. 41921001), the Fundamental Research Funds for Central Nonprofit Scientific Institution (grant no. 1610132020014) and the Open Fund of the State Key Laboratory of Remote Sensing Science (grant no. OFSLRSS201910).

References

Benali, A., Carvalho, A., Nunes, J., Carvalhais, N., and Santos, A.: Estimating air surface temperature in Portugal using MODIS LST data, Remote Sensing of Environment, 124, 108–121, https://doi.org/10.1016/j.rse.2012.04.024, 2012.

Bolstad, P., Swift, L., Collins, F., and Régnière, J.: Measured and predicted air temperatures at basin to regional scales in the southern Appalachian mountains, Agricultural and Forest Meteorology, 91, 161–176, https://doi.org/10.1016/S0168-1923(98)00076-8, 1998.

Caesar, J., Alexander, L., and Vose, R.: Large-scale changes in observed daily maximum and minimum temperatures: Creation and analysis of a new gridded data set, Journal of geophysical research atmospheres, 111, 1–10, https://doi.org/10.1029/2005jd006280, 2006.

Cao, M., Mao, K., Yan, Y., Shi, J; Wang, H., Xu, T., Fang, S., and Yuan, Z.: A new global gridded sea surface temperature data product based on multisource data, Earth System Science Data, 13, 2111–2134, https://doi.org/10.5194/ESSD-13-2111-2021, 2021.

Cesaraccio, C., Spano, D., Duce, P., and Snyder, R.: An improved model for determining degree-

https://doi.org/10.5194/essd-2021-309
Preprint. Discussion started: 20 October 2021

670 day values from daily temperature data, International Journal of Biometeorology, 45, 161–169, https://doi.org/10.1007/s004840100104, 2001.

Chen, F., Liu, Y., Liu, Q., and Qin, F.: A statistical method based on remote sensing for the estimation of air temperature in China, International Journal of Climatology, 35, 2131–2143, https://doi.org/10.1002/joc.4113, 2014.

675 Cristobal, J., Ninyerola, M., Pons, X., and Pla, M.: Improving Air Temperature Modelization by Means of Remote Sensing Variables, 2006 IEEE International Symposium on Geoscience and Remote Sensing, 2251–2254, https://doi.org/10.1109/IGARSS.2006.582, 2006.

Dee, D., Uppala, S., Simmons, A., Berrisford, P., Poli, P., Kobayashi, S., Andrae, U., Balmaseda, M., Balsamoa, G., Bauer, P., Bechtold, P., Beljaars, A., Berg, L., Bidlot, J., Bormann, N., Delsol,

680 C., Dragani, R., Fuentes, M., Geer, A., Haimberger, L., Healy, S., Hersbach, H., Hólm, E., Isaksen, L., Kållberg, P., Köhler, M., Matricardi, M., McNally, A., Monge-Sanz, B., Morcrette, J., Park, B., Peubey, C., Rosnay, P., Tavolato, C., Thépaut, J., and Vitart, F.: The ERA-Interim reanalysis: Configuration and performance of the data assimilation system, Quarterly Journal of the Royal Meteorological Society, 137, 553–597, https://doi.org/10.1002/qj.828, 2011.

685 Deng, X., Zhai, P., and Yuan, C.: Comparison and analysis of several sets of foreign reanalysis data, Meteorological Science and Technology, 38, 1–8, https://doi.org/10.19517/j.1671-6345.2010.01.001, 2010.

Ding, Y., Ren, G., Shi, G., Gong, P., Zheng, X., Zhai, P., Zhang, D., Zhao, Z., Wang, S., Wang, H., Luo, Y., Chen, D., Gao, X., and Dai, X.: China's National Assessment Report on Climate

690 Change (I): Climate change in China and the future trend, Climate Change Research, 2, 3–8, https://doi.org/10.3969/j.issn.1673-1719.2007.z1.001, 2006.

Du, J., Li, K., He, Z., Chen, L., Lin, P., and Zhu, X.: Daily minimum temperature and precipitation control on spring phenology in arid-mountain ecosystems in China, International Journal of Climatology, 40, 2568–2579, https://doi.org/10.1002/joc.6351, 2020.

695 Fang, S., Mao, K., Xia, X., Wang, P., Shi, J., M. Bateni, S., Xu, T., Cao, M., and Heggy, E.: A dataset of daily near-surface air temperature in China from 1979 to 2018 (Version 1.0) [Dataset], Zenodo, https://doi.org/10.5281/zenodo.5502275, 2021.

Floyd, R. and Braddock, R.: A simple method for fitting average diurnal temperature curves,

https://doi.org/10.5194/essd-2021-309
Preprint. Discussion started: 20 October 2021

Agricultural and Forest Meteorology, 32, 107–119, https://doi.org/10.1016/0168-1923(84)90081-9, 1984.

Gao, L., Bernhardt, M., and Schulz, K.: Elevation correction of ERA-Interim temperature data in complex terrain, Hydrology and Earth System Sciences, 16, 4661–4673, https://doi.org/10.5194/hess-16-4661-2012, 2012.

Gao, L., Lu, H., and Chen, W.: Evaluation of ERA-Interim Monthly Temperature Data over the Tibetan Plateau. Journal of Mountain Science, 11, 1154–1168, https://doi.org/10.1007/s11629-014-3013-5, 2014.

Gao, L., Wei, J., Wang, L., Bernhardt, M., Schulz, K., and Chen, X.: A high-resolution air temperature data set for the Chinese Tian Shan in 1979–2016, Earth System Science Data, 10, 2097–2114, https://doi.org/10.5194/essd-10-2097-2018, 2018.

Ge, Y.: Robust estimation by the least square method of regeneration rights, Bulletin of Surveying and Mapping, 8, 36–39, https://doi.org/10.13474/j.cnki.11-2246.2014.0254, 2015.

Han, S., Liu, B., Shi, C., Liu, Y., Qiu, M., and Sun, S.: Evaluation of CLDAS and GLDAS Datasets for Near-Surface Air Temperature over Major Land Areas of China, 12, 1–19, https://doi.org/10.3390/su12104311, 2020.

He, J.: Development of A Surface Meteorological Dataset of China with High Temporal and Spatial Resolution, Institute of Tibetan Plateau Research, CAS, http://ir.itpcas.ac.cn:8080/handle/131C11/1324, 2010.

He, J., Yang, K., Tang, W., Lu, H., Qin, J., Chen, Y., and Li, X.: The first high-resolution meteorological forcing dataset for land process studies over China, Scientific data, 7, 1–11, https://doi.org/10.1038/s41597-020-0369-y, 2020.

He, Y. and Wang, K.: Contrast patterns and trends of lapse rates calculated from near-surface air and land surface temperatures in China from 1961 to 2014, Science Bulletin, 65, 1217–1224, https://doi.org/10.1016/j.scib.2020.04.001, 2020.

Hersbach, H., Bell, B., Berrisford, P., Hirahara, S., Horányi, A., Muñoz-Sabater, J., Nicolas, J., Peubey, C., Radu, R., Schepers, D., Simmons, A., Soci, C., Abdalla, S., Abellan, X., Balsamo, G., Bechtold, P., Biavati, G., Bidlot, J., Bonavita, M., Chiara, G., Dahlgren, P., Dee, D., Diamantakis, M., Dragani, R., Flemming, J., Forbes, R., Fuentes, M., Geer, A., Haimberger, L.,

https://doi.org/10.5194/essd-2021-309
Preprint. Discussion started: 20 October 2021

Healy, S., Hogan, R., Hólm, E., Janisková, M., Keeley, S., Laloyaux, P., Lopez, P., Lupu, C., Radnoti, G., Rosnay, P., Rozum, I., Vamborg, F., Villaume, S., and Thépaut, J.: The ERA5 global reanalysis, Progress in Meteorological Science and Technology, 10, 1999–2049, https://doi.org/10.1002/qj.3803, 2020.

Jiang, F., Bremer, U., Arigony-Neto, J., Rosa, C., Jr, C., Costi, J., Freitas, M., and Schardong, F.: Comparison between Atmospheric Reanalysis Models ERA5 and ERA-Interim at the North Antarctic Peninsula Region, Annals of the American Association of Geographers, 111, 1147–1159, https://doi.org/10.1080/24694452.2020.1807308, 2021.

Jiang, H., Wen, D., Li, N., Ding, Y., and Xiao, J.: A new simulation method for the diurnal variation of temperature-sub-sine simulation, Meteorology and disaster reduction Research, 33, 61–65, https://doi.org/10.3969/j.issn.1007-9033.2010.03.010, 2010.

Johnson, M. and Fitzpatrick, E.: A comparison of two methods of estimating a mean diurnal temperature curve during the daylight hours, Theoretical and Applied Climatology, 25, 251–263, https://doi.org/10.1007/BF02243056, 1977.

Kharin, V., Zwiers, F., Zhang X., and Hegerl, G.: Changes in Temperature and Precipitation Extremes in the IPCC Ensemble of Global Coupled Model Simulations, Journal of Climate, 20, 1419–1444, https://doi.org/10.1175/JCLI4066.1, 2007.

Kobayashi, S., Ota, Y., Harada, Y., Ebita, A., Moriya, M., Onoda, H., Onogi, K., Kamahori, H., Kobayashi, C., Endo, H., Miyaoka, K., and Takahashi, K.: The JRA-55 Reanalysis: General Specifications and Basic Characteristics, Journal of the Meteorological Society of Japan, 93, 5–48, https://doi.org/10.2151/jmsj.2015-001, 2015.

Kong, F.: Spatial-temporal differentiation-based evolution characteristics of different extreme air temperature indexes in China from 1961 to 2018, Water Resources and Hydropower Engineering, 51, 67–80, https://doi.org/10.13928/j.cnki.wrahe.2020.04.008, 2020.

Lei, Y., Letu, H., Shang, H., and Shi, J.: Cloud cover over the Tibetan Plateau and eastern China: a comparison of ERA5 and ERA-Interim with satellite observations, Climate Dynamics, 54, 2941–2957, https://doi.org/10.1007/s00382-020-05149-x, 2020.

Leuning, R., Kelliher, F., Depury, D., and Schulze, E.: Leaf nitrogen, photosynthesis, conductance and transpiration-scaling from leaves to canopies, Plant, Cell & Environment, 18, 1183–1200,

https://doi.org/10.5194/essd-2021-309
Preprint. Discussion started: 20 October 2021

https://doi.org/10.1111/j.1365-3040.1995.tb00628.x, 1995.

Liao, Z.: Extreme cold events and interdiural temperature variation at the regional scale in China under global warming background, Chinese Academy of Meteorological Sciences, https://doi.org/10.27631/d.cnki.gzqky.2020.000003, 2020.

Lin, S., Nathan, M., Joseph, M., Mark, D., and Wu, J.: Evaluation of estimating daily maximum and minimum air temperature with MODIS data in east Africa, International Journal of Applied Earth Observation and Geoinformation, 18, 128–140, https://doi.org/10.1016/j.jag.2012.01.004, 2012.

Mao, K., Tang, H., Wang, X., Zhou, Q., and Wang, D.: Near-surface air temperature estimation from ASTER data based on neural network algorithm, International Journal of Remote Sensing, 20, 6021-6028, http://dx.doi.org/10.1080/01431160802192160, 2008.

Mao, K., Ma, Y., Tan, X., Shen, X., Liu, G., Li, Z., Chen, J., and Xia, L.: Global surface temperature change analysis based on MODIS data in recent twelve years, Advances in Space Research, 59, 503–512, https://doi.org/10.1016/j.asr.2016.11.007, 2016.

Meng, X., Guo, J., and Han, Y.: Preliminarily assessment of ERA5 reanalysis data. Journal of Marine Meteorology, 38, 91–99, https://doi.org/10.19513/j.cnki.issn2096-3599.2018.01.011, 2018.

Miao, C., Sun, Q., Duan, Q., and Wang, Y.: Joint analysis of changes in temperature and precipitation on the Loess Plateau during the period 1961–2011, Climate Dynamics, 47, 3221–3234, https://doi.org/10.1007/s00382-016-3022-x, 2016.

Mo, Z., Huang, L., Guo, X., Huang, L., Liu, L., Pang, Z., and Deng, Y.: Accuracy Analysis of GNSS Water Vapor Retrieval in Guilin area using ERA5 data, Journal of Nanjing University of Information Science & Technology (Natural Science Edition), 13, 131–137, https://doi.org/10.13878/j.cnki.jnuist.2021.02.001, 2021.

Mostovoy, G., King, R., Reddy, K., Kakani, V., and Filippova, M.: Statistical Estimation of Daily Maximum and Minimum Air Temperatures from MODIS LST Data over the State of Mississippi, GIScience & Remote Sensing, 43, 78–110, https://doi.org/10.2747/1548-1603.43.1.78, 2006.

Perkins, S., Pitman, A., Holbrook, N., and McAneney, J.: Evaluation of the AR4 Climate Models'

https://doi.org/10.5194/essd-2021-309
Preprint. Discussion started: 20 October 2021

Simulated Daily Maximum Temperature, Minimum Temperature, and Precipitation over Australia Using Probability Density Functions, Journal of Climate, 20, 4356–4376, https://doi.org/10.1175/JCLI4253.1, 2007.

Qiu, C. and Jiang, Y.: Design of production configuration parameters modeling system based on least square method, Modern Electronics Technique, 44, 83–87, https://doi.org/10.16652/j.issn.1004-373x.2021.04.018, 2021.

Ren, S., Deng, M., and Li, L.: Analysis on the occurrence time of Daily extreme temperature in Kaiping City, Guangdong Meteorology, 33, 35–36, https://doi.org/10.3969/j.issn.1007-6190.2011.04.008, 2011.

Ryoo, S., Kwon, W., and Jhun, J.: Characteristics of wintertime daily and extreme minimum temperature over South Korea, International Journal of Climatology, 24, 145–160, https://doi.org/10.1002/joc.990, 2010.

Schaer, C., Vidale, P., Luethi, D., Frei, C., Haeberli, C., Liniger, M., and Appenzeller, C.: The role of increasing temperature variability in european summer heatwaves. Nature, 427, 332–336., https://doi.org/10.1038/nature02300, 2004.

Schicker, I., Arias, D., and Seibert, P.: Influences of updated land-use datasets on WRF simulations for two Austrian regions, Meteorology and Atmospheric Physics, 2015, 128, 279–301, https://doi.org/10.1007/s00703-015-0416-y, 2015.

Schwingshackl, C., Hirschi, M., and Seneviratne, S.: Global Contributions of Incoming Radiation and Land Surface Conditions to Maximum Near-Surface Air Temperature Variability and Trend, Geophysical Research Letters, 45, 5034–5044, https://doi.org/10.1029/2018GL077794, 2018.

Serrano-Notivoli, R., Beguería, S., and Luis, M.: STEAD: a high-resolution daily gridded temperature dataset for Spain, Earth System Science Data, 11, 1171–1188, https://doi.org/10.5194/essd-11-1171-2019, 2019.

Tang, G., Clark, M., Newman, A., Wood, A., Papalexiou, S., Vionnet, V., and Whitfield, P.: SCDNA: a serially complete precipitation and temperature dataset for North America from 1979 to 2018, Earth System Science Data, 12, 2381–2409, https://doi.org/10.5194/essd-12-2381-2020, 2020.

Taszarek, M., Allen, J., Marchio, M., and Brooks, H.: Global climatology and trends in convective

https://doi.org/10.5194/essd-2021-309
Preprint. Discussion started: 20 October 2021

environments from ERA5 and rawinsonde data, npj Climate and Atmospheric Science, 4, 1–11, https://doi.org/10.1038/s41612-021-00190-x, 2021.

Tencer, B., Rusticucci, M., Jones, P., and Lister, D.: A Southeastern South American Daily Gridded Dataset of Observed Surface Minimum and Maximum Temperature for 1961–2000. Bulletin of the American Meteorological Society, 92, 1339–1346, https://doi.org/10.1175/2011BAMS3148.1, 2011.

Tomasz, B., Mateusz, S., Ignacy, K., Robert, M., Tomasz, O., Abdelkader, M., and Mikołaj, P.: CPLFD–GDPT5: High-resolution gridded daily precipitation and temperature data set for two largest Polish river basins, Earth System Science Data, 8, 127–139, https://doi.org/10.5194/essd-8-127-2016, 2016.

Wang, C.: Determination of AWS Climate Thresholds by Using Altitude Correction Method, Meteorological Science and Technology, 41, 93–96, https://doi.org/10.3969/j.issn.1671-6345.2013.01.018, 2013.

Wang, L., Zhang, X., Fang, Y., and Xia, D.: Applicability Assessment of China Meteorological Forcing Dataset in Upper Yangtze River Basin, Water Power, 43, 18–22, https://doi.org/10.3969/j.issn.0559-9342.2017.03.005, 2017.

Wen, X.: Time series modeling and analysis of remotely sensed land surface temperature over the Tibetan plateau, University of Electronic Science and Technology of China, 1, 1–91, https://doi.org/10.27005/d.cnki.gdzku.2020.000994, 2020.

Xing, L., Li, J., and Jiao, W.: Estimation of daily maximum and minimum temperature of Lanzhou City based on MODIS and Random forest, Arid Zone Research, 37, 152–158, https://doi.org/10.13866/j.azr.2020.03.17, 2020.

Xu, W., Sun, R., Zhou, S., Jin, Z., and Hu, B.: Estimating daily maximum and minimum air temperatures by remote sensing and GIS, Journal of Beijing Normal University (Natural Science), 53, 344–350, https://doi.org/10.16360/j.cnki.jbnuns.2017.03.016, 2017.

Yan, Y., Mao, K., Shi, J., Piao, S., Shen, X., Dozier, J., Liu, Y., Ren, H., and Bao, Q.: Driving forces of land surface temperature anomalous changes in North America in 2002–2018, Scientific Reports, 10, 1–13, https://doi.org/10.1038/s41598-020-63701-5, 2020.

Yang, K., He, J., Tang, W., Qin, J., and Cheng, C.: On downward shortwave and longwave

https://doi.org/10.5194/essd-2021-309
Preprint. Discussion started: 20 October 2021

radiations over high altitude regions: Observation and modeling in the Tibetan Plateau, Agricultural and Forest Meteorology, 150, 38–46, https://doi.org/10.1016/j.agrformet.2009.08.004, 2010.

Yang, K. and He, J.: China meteorological forcing dataset (1979-2018), National Tibetan Plateau Data Center, https://doi.org/10.11888/AtmosphericPhysics.tpe.249369.file, 2019.

Yoo, C., Im, J., Park, S., and Quackenbushb, L.: Estimation of daily maximum and minimum air temperatures in urban landscapes using MODIS time series satellite data, ISPRS Journal of Photogrammetry and Remote Sensing, 137, 149–162, https://doi.org/10.1016/j.isprsjprs.2018.01.018, 2018.

Zhang, G., Yang, L., Qu, M., and Chen, H.: Interpolation of daily mean temperature by using geographically weighted regression-Kriging, Chinese Journal of Applied Ecology, 26, 1531–1536, https://doi.org/10.13287/j.1001-9332.20150302.004, 2015.

Zhang, X., Huang, L., Quan, Q., Zhang, L., Shen, B., and Mo, S.: Relationship of vegetation cover change with climate factors in source region of the Yellow River based on ITPCAS forcing data. Journal of Northwest Sci-Tech University of Agriculture and Forestry: Natural Science Edition, 47, 55–68, https://doi.org/10.13207/j.cnki.jnwafu.2019.09.007, 2019.

Zhang, Y., Gao, Z., Pan, Z., Li, D., and Huang, X.: Spatiotemporal variability of extreme temperature frequency and amplitude in China-ScienceDirect, Atmospheric Research, 185, 131–141, https://doi.org/10.1016/j.atmosres.2016.10.018, 2017.

Zhao, B., Mao, K., Cai, Y., Shi, J., Li Z., Qin, Z., and Meng, X.: A combined Terra and Aqua MODIS land surface temperature and meteorological station data product for China from 2003 to 2017, Earth System Science Data, 12, 2555–2577, https://doi.org/10.5194/essd-12-2555-2020, 2020.

Zhao J. and Duan, Z.: Occurrence of Maximum and Minimum Temperature, Meteorological and Environmental Sciences, 37, 86–89, https://doi.org/10.16765/j.cnki.1673-7148.2014.04.012, 2014.

Zhu, W., Lű, A., and Jia, S.: Estimation of daily maximum and minimum air temperature using MODIS land surface temperature products, Remote Sensing of Environment, 130, 62–73, https://doi.org/10.1016/j.rse.2012.10.034, 2013.